

Domain growth in cholesteric blue phases: hybrid lattice Boltzmann simulations

O. Henrich, D. Marenduzzo, K. Stratford, M. E. Cates

SUPA, School of Physics, University of Edinburgh, Mayfield Road Edinburgh EH9 3JZ, Scotland

Abstract

Here we review a hybrid lattice Boltzmann algorithm to solve the equations of motion of cholesteric liquid crystals. The method consists in coupling a lattice Boltzmann solver for the Navier-Stokes equation to a finite difference method to solve the dynamical equations governing the evolution of the liquid crystalline order parameter. We apply this method to study the growth of cholesteric blue phase domains, within a cholesteric phase. We focus on the growth of blue phase II and on a thin slab geometry in which the domain wall is flat. Our results show that, depending on the chirality, the growing blue phase is either BPII with no or few defects, or another structure with hexagonal ordering. We hope that our simulations will spur further experimental investigations on quenches in micron-size blue phase samples. The computational size that our hybrid lattice Boltzmann scheme can handle suggest that large scale simulations of new generation of blue phase liquid crystal device are within reach.

Key words: lattice Boltzmann simulations, liquid crystals, cholesterics, blue phases

PACS: 64.70.mf, 61.30.Mp, 61.30.-v

2000 MSC: 76M20, 76M25, 82-08

1. Introduction

The lattice Boltzmann (LB) algorithm [1, 2] is a powerful method to solve the Navier-Stokes equations of ideal and complex fluids, which, due to its conceptual simplicity and ease to code, provides an attractive alternative to other methods more commonly adopted in computational fluids dynamics,

such as e.g. finite elements algorithms. In the last couple of decades, the LB method has evolved to a powerful tool to study a variety of problems in complex fluids [3, 4, 5, 6, 7, 8, 9, 10, 11, 12, 13, 14]. In this respect, particularly successful avenues have been, among others, the study of binary fluids and of liquid crystals.

The original LB method to solve the hydrodynamic equations of motion of complex fluids typically consisted of introducing extra distribution function, which evolved via an LB dynamics determined by an appropriate collision kernel. These distribution functions control the dynamics of conserved or non-conserved order parameters which is coupled to the fluid momentum, itself governed by the primary LB distribution function. The Chapman-Enskog expansion of such dynamics then gave back the continuum hydrodynamic equations for the coupled system. However, on top of introducing some systematic, albeit small, errors, this “full LB” approach had the drawback of requiring a large memory to store all the distribution functions for the whole lattice. This turned out to be particularly severe for the case of liquid crystal, where the order parameter (in the Beris-Edwards model [15]) is a traceless and symmetric tensor, and therefore required the introduction of five extra sets of distribution functions. This leads to high memory requirements which ultimately limits the size of the lattice to be studied. The new generation of LB studies for complex fluids has a growing need to be able to cope with larger and larger systems, to make best use of the potentially very good scalability of parallel LB codes. As a result, new hybrid algorithms have been coded and deployed, for both binary fluids and liquid crystals [9, 11, 16], where the LB algorithm is dedicated to solve the (forced) Navier-Stokes equation for momentum alone, and is coupled to a standard efficient finite-difference solver (e.g. a predictor corrector) for the order parameter dynamics. Hybrid LB simulations of binary fluids [9] and of active gel and active liquid crystal hydrodynamics and rheology [11, 12] have validated the hybrid algorithm through a comparison with full LB simulations, and have shown that this framework is potentially very flexible and robust. Here, after briefly reviewing the equations of motion of liquid crystal hydrodynamics and the hybrid LB approach which we use to solve them, we apply our algorithm to study the growth of domains in cholesteric blue phases (BPs).

BPs are a spectacular example of a soft solid, made up by a spontaneously occurring network of disclination lines in a cholesteric liquid crystal [17]. BPs appear very close to the transition between the isotropic and the cholesteric

phase. In a liquid crystal in the cholesteric phase, the director field, which quantifies the local direction of molecular ordering in the fluid, has the tendency to twist around an axis, which is that of the cholesteric helix. Close to the transition to the isotropic phase, a simple helical order is frustrated and it is more advantageous for the director field to rotate in a helical fashion around any axis perpendicular to a line - this director field pattern was named a "double twist cylinder". Mathematically, it is impossible to patch up different double twist cylinders without creating defects in between, and this is what gives rise to the disclination network making up BPs.

Without an electric field, three different kinds of BPs are found. BPI and BPII are cubic phases characterised by a regular disclination line lattice: in BPI the double twist cylinders are arranged in a simple cubic lattice, whereas in BPII they form a body-centred cubic lattice. BPIII, or the "blue fog", is not a cubic phase, and its structure is not fully understood to date: the dominating view is that it is a structure made up by double twisted cylinders arranged in an irregular way [17].

As the period of the BP network and the timescales of response to an applied perturbation are in the sub- μm and sub- μs range respectively, these soft materials are promising candidates for tunable photonic crystals and a new generation of fast liquid crystal devices. Recent experiments [18] managed to stabilize BPs over a strikingly wide temperature range of 50 K, compared to the precedingly narrow temperature range of about 1 K, putting these technological advances now within reach. However, in order for this exciting potential to be fully realised, our understanding of BPs needs to become as quantitative as the one we have for conventional nematic liquid crystal displays.

From a more fundamental physics points of view, BPs are remarkable materials. A series of very interesting experiments [19, 20, 21] have shown for instance that BP droplets facet when they nucleate and grow inside another isotropic fluid. BP droplets, like other fluids, may also wet a surface, but due to their elastic properties their surface shows steps and may reconstruct, like that of a solid. According to the current understanding, the underlying disclination meshwork is primarily cause of this highly non-trivial phenomenology, as it behaves like an elastic network.

Existing simulations of BPs [22, 23, 24, 25] have significantly extended our quantitative understanding of their physics, which first rested on semi-analytical approximations (see e.g. [26]). For instance, obtaining the shape of the phase diagram, with BPI and BPII appearing in the experimentally

observed order upon increasing the chirality [22, 23], as well as understanding the presence of anomalous electrostriction in BPI under an electric field [25], were only possible with extensive simulations of these structures. However, these simulations have thus far been limited to one unit cell, within which several disclination cores are present and require a fine enough discretisation to be correctly resolved. By necessity, this approach leaves out a number of physically relevant supra-unit cell phenomena such as the possibility of large scale lattice reconstructions (perhaps induced by shear or by an applied field), and the appearance of defects or spatial inhomogeneities in the BP lattice. Furthermore, the length scale covered by simulations is much smaller than the ones relevant for either the domain growth experiments or BP devices. As a first step to model more realistic situations, we present here supra-unit cell large scale 3D simulations of the domain growth of BP domains in cholesteric and isotropic liquid crystals.

Our hybrid lattice Boltzmann results suggest that the physics of BP domain growth is highly non-trivial. Focussing on a thin slab geometry, we observe below qualitatively different growth dynamics of BP domains inside cholesterics, for different values of the chirality. For large values of this parameter, we find that BPII domains growing inside a cholesteric evolve into a different disclination network, which possesses local hexagonal symmetry. Further simulations in an isotropic fluid show the same transition, although the growth kinetics of the new BP phase is different. To aid comparison with potential future experiments, we also visualize the disclination network and simulate the appearance of the sample under polarized light. The feasibility of such large scale simulations is promising in view of further future applications, e.g. to device modelling.

2. Model and methods

2.1. Equations of motion

Following the Beris-Edwards model for liquid crystal hydrodynamics [15], we describe the BPs by a traceless, symmetric, second rank order parameter tensor, \mathbf{Q} . The equilibrium thermodynamic properties are determined by a Landau - de Gennes free energy \mathcal{F} , whose density f is,

$$\begin{aligned}
 f = & \frac{A_0}{2} \left(1 - \frac{\gamma}{3}\right) Q_{\alpha\beta}^2 - \frac{A_0\gamma}{3} Q_{\alpha\beta} Q_{\beta\gamma} Q_{\gamma\alpha} + \frac{A_0\gamma}{4} (Q_{\alpha\beta}^2)^2 \\
 & + \frac{K}{2} (\epsilon_{\alpha\gamma\delta} \partial_\gamma Q_{\delta\beta} + 2q_0 Q_{\alpha\beta})^2.
 \end{aligned}
 \tag{1}$$

(Notice that in our notation Greek indices denote Cartesian components and summation over repeated indices is implied.) In Eq. 1 A_0 is a constant, K is an elastic constant (we adopt the one-constant-approximation), q_0 is $2\pi/p$, where p is the pitch of the cholesteric helix, while γ is a control parameter linked to the temperature for thermotropic liquid crystals, or concentration for lyotropic ones. Increasing γ leads to an increase in the average magnitude of order. The local magnitude of order, $q(\vec{r})$, is the largest eigenvalue of \mathbf{Q} . This quantity is also used to identify disclination lines: when the local magnitude of order falls below a predetermined threshold, we identify that lattice point as constituting part of a disclination. This prescription is very easy to implement and allows an accurate determination of the disclinations. Changing the numerical value of the threshold generally leads to a change in the thickness of the disclination tubes. For our study, we have typically chosen a threshold of $q = 0.19$ for defect/disclination identification. The Beris-Edwards equations for the evolution of the \mathbf{Q} -tensor, which we aim to solve, are [15]

$$D_t \mathbf{Q} = \Gamma \left(\frac{-\delta \mathcal{F}}{\delta \mathbf{Q}} + \frac{1}{3} \text{Tr} \left(\frac{\delta \mathcal{F}}{\delta \mathbf{Q}} \right) \mathbf{I} \right) \equiv \Gamma \mathbf{H}. \quad (2)$$

Here Γ is a collective rotational diffusion constant, while $\frac{\delta}{\delta \mathbf{Q}}$ indicates the functional derivative with respect to the tensor order parameter. Tr stands for trace, and D_t is the material derivative for rod-like molecules [15]:

$$D_t \mathbf{Q} \equiv (\partial_t + \vec{u} \cdot \nabla) \mathbf{Q} - \mathbf{S}(\mathbf{W}, \mathbf{Q}) \quad (3)$$

$$\begin{aligned} \mathbf{S}(\mathbf{W}, \mathbf{Q}) &\equiv (\xi \mathbf{D} + \omega)(\mathbf{Q} + \mathbf{I}/3) \quad (4) \\ &+ (\mathbf{Q} + \mathbf{I}/3)(\xi \mathbf{D} - \omega) - 2\xi(\mathbf{Q} + \mathbf{I}/3)\text{Tr}(\mathbf{Q}\mathbf{W}), \end{aligned}$$

where \mathbf{D} and ω are the symmetric and the anti-symmetric part respectively of the velocity gradient tensor $W_{\alpha\beta} = \partial_\beta u_\alpha$ [15, 10], \vec{u} being the velocity field.

Eq. 2 may be mathematically derived from an underlying microscopic model via a Poisson brackets approach [15]. Physically, this equation means that the system tries to evolve, in the absence of any flow or backflow ($\vec{u} = 0$), so as to minimise its free energy. This is ensured by the presence of the molecular field, \mathbf{H} . The presence of a non-zero \vec{u} requires one to substitute the usual partial derivative ∂_t with the material derivative D_t , which describes advection by the fluid velocity (the term $\vec{u} \cdot \nabla \mathbf{Q}$), and also includes a further coupling $\mathbf{S}(\mathbf{W}, \mathbf{Q})$ between the velocity gradient tensor and the order parameter, which arises due to the tensorial nature of the latter. Physically, $\mathbf{S}(\mathbf{W}, \mathbf{Q})$ appears because the order parameter distribution can be both ro-

tated and stretched by flow gradients [15]. Mathematically, $\mathbf{S}(\mathbf{W}, \mathbf{Q})$ contains a (phenomenological) mixture of upper and lower convected derivatives. This is similar to what is done in other hydrodynamic equations for polymeric fluids, such as the Johnson-Segalman model [27]. The term ξ , which may be also viewed as a parameter controlling the weights of the lower and upper convected derivatives, is related to the aspect ratio of the molecules. This parameter controls whether the director field is flow aligning in shear flow ($\xi \geq 0.6$), creating a stable response, as opposed to flow tumbling, which gives an unsteady response ($\xi < 0.6$).

The fluid velocity, \vec{u} , obeys the continuity equation of an incompressible fluid, and the Navier-Stokes equation,

$$\begin{aligned} \rho(\partial_t + u_\beta \partial_\beta)u_\alpha &= \partial_\beta(\Pi_{\alpha\beta}) + \eta\partial_\beta(\partial_\alpha u_\beta + \partial_\beta u_\alpha) \\ &+ (1 - 3\partial_\rho P_0)\partial_\gamma u_\gamma \delta_{\alpha\beta}, \end{aligned} \quad (5)$$

where ρ is the fluid density, η is an isotropic viscosity. The stress tensor $\Pi_{\alpha\beta}$ consists of a symmetric part $\sigma_{\alpha\beta}$ and an antisymmetric contribution $\tau_{\alpha\beta}$,

$$\Pi_{\alpha\beta} = \sigma_{\alpha\beta} + \tau_{\alpha\beta} \quad (6)$$

$$\begin{aligned} \sigma_{\alpha\beta} &= -P_0\delta_{\alpha\beta} + 2\xi(Q_{\alpha\beta} + \frac{1}{3}\delta_{\alpha\beta})Q_{\gamma\epsilon}H_{\gamma\epsilon} \\ &- \xi H_{\alpha\gamma}(Q_{\gamma\beta} + \frac{1}{3}\delta_{\gamma\beta}) - \xi(Q_{\alpha\gamma} + \frac{1}{3}\delta_{\alpha\gamma})H_{\gamma\beta} \\ &- \partial_\alpha Q_{\gamma\nu} \frac{\partial f}{\partial Q_{\gamma\nu,\beta}} \end{aligned} \quad (7)$$

$$\tau_{\alpha\beta} = Q_{\alpha\gamma}H_{\gamma\beta} - H_{\alpha\gamma}Q_{\gamma\beta}, \quad (8)$$

where $P_0 = \rho T - f$ is an isotropic pressure [15] and $Q_{\gamma\nu,\beta} = \partial_\beta Q_{\gamma\nu}$.

In our simulations, the coupling to hydrodynamics via a non-trivial pressure tensor can be switched off, essentially by imposing a constant zero velocity profile. In this way the effects of flow and backflow may be unambiguously pinpointed. In our case, backflow does not dramatically modify the kinetic pathway through which BP domains grow, but it renders the dynamics faster. Similar effects have been seen on the switching dynamics and on the rheological properties of BPs [24, 25].

The equilibrium phase diagrams of BPs are commonly expressed as a

function of the chirality κ and reduced temperature τ , defined [22, 23, 26] as

$$\kappa = \sqrt{\frac{108L_1q_0^2}{A_0\gamma}} \quad (9)$$

$$\tau = \frac{27(1 - \gamma/3)}{\gamma}. \quad (10)$$

We selected $\tau = 0$ and varied κ in our simulations (reported in the Results section). For the other kinetic parameters, we chose $\Gamma = 0.3$, $\xi = 0.7$ (hence a flow aligning BP) and $\eta = 5/3$ (these choices are suggested by previous experience in blue phase numerics [24, 25]). Time and space is measured in simulation units in what follows.

2.2. The hybrid lattice Boltzmann algorithm

In order to solve Eqs. 2 and 5, as mentioned in the Introduction, we use here a hybrid lattice Boltzmann algorithm. The idea of the algorithm is simple. We observe that the coupling between the velocity field and the order parameter equation (see Eq. 2) is via the material derivative term, which requires both the velocity and the velocity gradient fields. On the other hand, the order parameter field affects the Navier-Stokes equation through the pressure tensor $\Pi_{\alpha\beta}$. Our hybrid lattice Boltzmann approach consists in solving Eq. 2 via a finite-difference predictor-corrector algorithm, while the LB algorithm is devoted to the integration of Eq. 5. The order parameter and velocity fields are (sequentially) updated at every time step via these algorithms. The LB step requires as an input the order parameter field (hence the pressure tensor and its divergence), which is provided by the finite difference solver. On the other hand, the LB algorithm updates the velocity field which is then in turn required by the finite difference scheme to further evolve the dynamics of the order parameter. Due to the limited required coupling between LB and finite difference algorithms, this hybrid approach could be generalised to a variety of hydrodynamic equations of motion involving the dynamics of an order parameter besides the Navier-Stokes equations [9, 11, 16]. As mentioned above, a similar hybrid approach has indeed already been successfully used for a binary fluid as well [9, 16].

With respect to a full LB approach [28, 10], the primary advantage of this hybrid method is that it will allow simulations of larger systems as it involves consistently smaller memory requirements. Indeed, while in a full LB treatment one has to store 6 sets of 15 distribution functions at any

lattice point (if we choose the 3DQ15 velocity vector lattice [1] as we do here), in the hybrid approach just one set of distribution functions plus the five independent components of the \mathbf{Q} tensor are needed. The hybrid method should also be numerically more stable since it avoids the error term arising in the Chapman-Enskog expansion used to connect the LB model to the order parameter evolution equation in the continuum limit [28]. Finally, it should be possible to include noise in a conceptually simpler way as one can in principle couple a noisy LB dynamics, for which precise prescriptions exist [29], for the Navier-Stokes equation with a Langevin dynamics for the order parameter(s) evolution. In the present work, however, we neglect noise. Thus our treatment couples a mean-field dynamics of the cholesteric order to a noiseless classical fluid.

Let us describe first how to integrate the Navier-Stokes equations with a slightly modified standard Lattice Boltzmann algorithm [28]. This is defined in terms of a single set of partial distribution functions, the scalars $f_i(\vec{x})$, that sum on each lattice site \vec{x} to give the density. (Note that f without Latin index is the free energy density from Eq. 1.) Each f_i is associated with a lattice vector \vec{e}_i [28, 10]. We choose a 15-velocity model on the cubic lattice with lattice vectors:

$$\vec{e}_i^{(0)} = (0, 0, 0) \tag{11}$$

$$\vec{e}_i^{(1)} = (\pm 1, 0, 0), (0, \pm 1, 0), (0, 0, \pm 1) \tag{12}$$

$$\vec{e}_i^{(2)} = (\pm 1, \pm 1, \pm 1). \tag{13}$$

The indices, i , are ordered so that $i = 0$ corresponds to $\vec{e}_i^{(0)}$, $i = 1, \dots, 6$ correspond to the $\vec{e}_i^{(1)}$ set and $i = 7, \dots, 14$ to the $\vec{e}_i^{(2)}$ set.

Physical variables are defined as moments of the distribution functions:

$$\rho = \sum_i f_i, \quad \rho u_\alpha = \sum_i f_i e_{i\alpha}. \tag{14}$$

The distribution functions evolve in a time step Δt according to

$$f_i(\vec{x} + \vec{e}_i \Delta t, t + \Delta t) - f_i(\vec{x}, t) = \frac{\Delta t}{2} [\mathcal{C}_{f_i}(\vec{x}, t, \{f_i\}) + \mathcal{C}_{f_i}(\vec{x} + \vec{e}_i \Delta t, t + \Delta t, \{f_i^*\})]. \tag{15}$$

This represents free streaming with velocity \vec{e}_i followed by a collision step which allows the distributions to relax towards equilibrium. The f_i^* 's are first order approximations to $f_i(\vec{x} + \vec{e}_i dt, t + dt)$, and they are obtained by

using $\Delta t \mathcal{C}_{f_i}(\vec{x}, t, \{f_i\})$ on the right hand side of Eq. (15). Discretizing in this way, which is similar to a predictor-corrector scheme, has the advantages that lattice viscosity terms are eliminated to second order and that the stability of the scheme is improved [28].

The collision operators are taken to have the form of a single relaxation time Boltzmann equation, together with a forcing term

$$\mathcal{C}_{f_i}(\vec{x}, t, \{f_i\}) = -\frac{1}{\tau_f}(f_i(\vec{x}, t) - f_i^{eq}(\vec{x}, t, \{f_i\})) + p_i(\vec{x}, t, \{f_i\}), \quad (16)$$

The form of the equations of motion follow from the choice of the moments of the equilibrium distributions f_i^{eq} and the driving terms p_i . Note that f_i^{eq} is constrained by

$$\sum_i f_i^{eq} = \rho, \quad \sum_i f_i^{eq} e_{i\alpha} = \rho u_\alpha, \quad \sum_i f_i^{eq} e_{i\alpha} e_{i\beta} = -\sigma_{\alpha\beta} + \rho u_\alpha u_\beta, \quad (17)$$

$$\sum_i f_i^{eq} e_{i\alpha} e_{i\beta} e_{i\gamma} = \frac{\rho \tau_f}{3} (u_\alpha \delta_{\beta\gamma} + u_\beta \delta_{\alpha\gamma} + u_\gamma \delta_{\alpha\beta}) \quad (18)$$

where the zeroth and first moments are chosen to impose conservation of mass and momentum. The second moment of f^{eq} is determined by $\sigma_{\alpha\beta}$, which is the symmetric part of the stress tensor $\Pi_{\alpha\beta}$, and does *not* include either the double gradient term, $\partial_\alpha Q_{\gamma\nu} \frac{\partial f}{\partial Q_{\gamma\nu,\beta}}$, or the $f \delta_{\alpha\beta}$ contribution from the isotropic pressure. The constraint on the third moment is necessary to get an isotropic Navier-Stokes equation via the Chapman-Enskog expansion of Eq. 15 (see e.g. [28]).

The divergences of $\tau_{\alpha\beta}$ and of $\partial_\alpha Q_{\gamma\nu} \frac{\partial f}{\partial Q_{\gamma\nu,\beta}}$ instead enter effectively as a body force and constrain the first moment of the driving terms p_i : this ensures that spurious velocities are eliminated, or greatly reduced, as we show below. The constraints on the p_i 's are [30]:

$$\sum_i p_i = 0, \quad \sum_i p_i e_{i\alpha} = \partial_\beta \tau_{\alpha\beta} - \partial_\beta \left(\partial_\alpha Q_{\gamma\nu} \frac{\partial f}{\partial Q_{\gamma\nu,\beta}} \right) + \partial_\alpha f \equiv b_\alpha, \quad (19)$$

$$\sum_i p_i e_{i\alpha} e_{i\beta} = 0, \quad \sum_i p_i e_{i\alpha} e_{i\beta} e_{i\gamma} = 0. \quad (20)$$

This scheme was inspired by the one used in Ref. [31] to reduce spurious velocities in a full LB binary fluid simulation. In the case of liquid crystals spurious velocities are equally eliminated by introducing the divergence of

$g_{\alpha\beta} = -\partial_\alpha Q_{\gamma\nu} \frac{\partial f}{\partial Q_{\gamma\nu,\beta}} + f\delta_{\alpha\beta}$. To see this, we transform $\partial_\beta g_{\alpha\beta}$ in the following way:

$$\begin{aligned}
& - \partial_\beta \left(\partial_\alpha Q_{\gamma\nu} \frac{\partial f}{\partial Q_{\gamma\nu,\beta}} \right) + \partial_\alpha f = \\
& - \partial_\beta \left(\frac{\partial f}{\partial Q_{\gamma\nu,\beta}} \right) \partial_\alpha Q_{\gamma\nu,\beta} - \frac{\partial f}{\partial Q_{\gamma\nu,\beta}} \partial_\alpha Q_{\gamma\nu,\beta} \\
& + \left(\frac{\partial f}{\partial Q_{\gamma\nu}} + \frac{\partial f}{\partial Q_{\gamma\nu,\beta}} \right) \partial_\alpha Q_{\gamma\nu} = -H_{\gamma\nu} \partial_\alpha Q_{\gamma\nu}, \tag{21}
\end{aligned}$$

where we introduced $H_{\gamma\nu}$ in the last line because the \mathbf{Q} tensor is traceless and therefore $Q_{\gamma\gamma} = 0$. We see that if we directly insert Eq. 21 as a body force this term vanishes in equilibrium as it is proportional to the molecular field. In this way spurious velocities, i.e. non-zero velocities in equilibrium due to the different discretisation of the pressure tensor and the molecular field, are in principle avoided. We have verified that this is the case numerically.

Conditions Eqs. 17 – 20 are satisfied by writing the equilibrium distribution functions and forcing terms as polynomial expansions in the velocity,

$$f_i^{eq} = A_s + B_s u_\alpha e_{i\alpha} + C_s u^2 + D_\alpha u_\alpha u_\beta e_{i\alpha} e_{i\beta} + E_{\alpha\beta} e_{i\alpha} e_{i\beta} + P_s b_\alpha e_{i\alpha}, \tag{22}$$

where $s \in \{0, 1, 2\} \Leftrightarrow \vec{e}_i^2 \in \{0, 1, 3\}$ identifies separate coefficients for different square absolute values of the velocities.

The coefficients in the expansion are determined by the requirements that all the constraints enumerated above, Eqs. 17,18,19 and 20, are fulfilled. A possible choice, which we adopt, is given below:

$$\begin{aligned}
A_2 &= \frac{\rho T}{10}, & A_1 &= A_2, & A_0 &= \rho - 14A_2, \\
B_2 &= \rho/24, & B_1 &= 8B_2, \\
C_2 &= -\frac{\rho}{24}, & C_1 &= 2C_2, & C_0 &= -\frac{2\rho}{3}, \\
D_2 &= \frac{\rho}{16}, & D_1 &= 8D_2 \\
E_{2\alpha\beta} &= -\frac{1}{16}(\Pi_{\alpha,\beta} - \frac{\sigma_{\gamma\gamma}}{3}\delta_{\alpha\beta}), & E_{1\alpha\beta} &= 8E_{2\alpha\beta} \\
P_2 &= \frac{1}{24}, & P_1 &= 8P_2. \tag{23}
\end{aligned}$$

Clearly the stress tensor $\Pi_{\alpha\beta}$ is a function of $Q_{\alpha\beta}$ and, in the hybrid approach, the coefficients $E_{2\alpha\beta}$ and $E_{1\alpha\beta}$ of the f_i^{eq} 's are computed by using the solution (via finite difference methods) of the coupled Eq. (2). This differs from the fully LB treatment of liquid crystals [28, 10].

2.3. Rendering of the optical pattern

Due to their anisotropic structure, liquid crystal molecules are optically active and cause polarisation rotations and phase-shifts in the electric field components of transmitted polarised light. A common experimental technique is to observe the transmission pattern under a microscope using a crossed-polariser geometry. Every molecule along the path of the incident beam acts as a retarder. Thus the transmission pattern can be regarded as an overall effect of the constituting molecules. It depends on the local orientation of the molecules, i.e. on the director field, the refractive-index anisotropy and on the shape of the domain.

While it is in general not trivial to infer the local director field from the transmission pattern, it is rather simple to simulate the latter from a given director field. To this end, we have employed the Müller matrix technique [32, 33], which simulates the light transmission signal observed in a micron-size sample under a pair of crossed polarisers. We calculated the polarised optical texture corresponding to the instantaneous director field of the growing BP domain and its surrounding environment. In our approach the director field $\vec{d}(\vec{r})$ is defined as the normalized eigenvector related to the largest eigenvalue of the order parameter tensor \mathbf{Q} . According to Stokes the polarisation state of the light can be conveniently described by a set of four parameters, combined in the 4-component Stokes vector $\vec{S} = (S_0, S_1, S_2, S_3)$. Its first component S_0 is proportional to the intensity of the light.

In order to simulate the retardation of a liquid crystal droplet one assumes the droplet of size L to consist of N equally thick liquid crystal layers with thickness $h = L/N$. The effect of each layer situated at the site \vec{r} onto the Stokes-vector \vec{S} is then described by the Müller matrix

$$M(\vec{r}) = \begin{pmatrix} 1 & 0 & 0 & 0 \\ 0 & c_b^2 + s_b^2 c_d & c_b s_b (1 - c_d) & -s_b s_d \\ 0 & c_b s_b (1 - c_d) & s_b^2 + c_b^2 c_d & c_b s_d \\ 0 & s_b s_d & -c_b s_d & c_d \end{pmatrix}, \quad (24)$$

where

$$c_b = \cos 2\beta(\vec{r}), \quad s_b = \sin 2\beta(\vec{r}), \quad c_d = \cos \delta(\vec{r}), \quad s_d = \sin \delta(\vec{r}) \quad (25)$$

and

$$\alpha(\vec{r}) = \arccos(d_z(\vec{r})), \quad (26)$$

$$\beta(\vec{r}) = \arctan(d_x(\vec{r})/d_y(\vec{r})), \quad (27)$$

$$\delta(\vec{r}) = \frac{2\pi q(\vec{r})h}{\lambda} \left(\frac{n_0 n_e}{\sqrt{n_0^2 \sin^2 \alpha(\vec{r}) + n_e^2 \cos^2 \alpha(\vec{r})}} - n_0 \right). \quad (28)$$

The quantity q is the local scalar order parameter defined as the largest eigenvalue of the order parameter tensor \mathbf{Q} , whereas λ gives the wavelength of the incident light. We set the ordinary and extraordinary refractive indices to $n_0 = 1.5$ and $n_e = 2.0$ respectively.

The above definitions of the angles α and β are correct for a light beam propagating along the z-direction. We assumed this throughout our analysis, but the adaption to other situations is straightforward. Generally, α is the angle between the direction of the light beam and the local director field, while β measures the angle between the projection of the local director field onto the coordinate plane perpendicular to the beam direction and a coordinate axis in that plane, in our case the x-axis. The crossed-polariser geometry is realized by two different Müller matrices of the type

$$P = \frac{1}{2} \begin{pmatrix} 1 & \cos \phi & \sin \phi & 0 \\ \cos \phi & \cos^2 \phi & \cos \phi \sin \phi & 0 \\ \sin \phi & \sin \phi \cos \phi & \sin^2 \phi & 0 \\ 0 & 0 & 0 & 0 \end{pmatrix}. \quad (29)$$

The parameter ϕ defines the angle between the polariser or analyzer and a coordinate axis perpendicular to the beam direction. For a right angled crossed-polariser setup one assumes for instance $\phi_{in} = 0$ for the polariser and $\phi_{out} = \pi/2$ for the analyser.

The total effect of the liquid crystal droplet on a Stokes vector \vec{S}_{in} can be formally expressed by a matrix product of consecutive Müller matrices, following the path of the light beam:

$$\vec{S}_{out}(x, y) = P_{out} \prod_{k=0}^N M(i = x/h, j = y/h, k) P_{in} \vec{S}_{in}(x, y). \quad (30)$$

The matrices $M(i, j, k)$ shall be understood as the discretised version of $M(\vec{r})$. As we are interested in the general appearance of the sample under polychromatic polarised light, we performed this operation for slightly different

wavelengths in the magnitude of the unit cell size of the BPs, which was 16 in lattice units, and weighted the results accordingly [34]. We simulated three different components with wavelengths $\lambda = 16, 18$ and 20 in lattice units and assigned them the weights $w = 0.2, 0.6$ and 0.2 respectively. This procedure can only be regarded as a simple approach to model white light. Nevertheless it proves to be sufficient as the results for different components with similar wavelengths differ only slightly in their brightness and only insignificantly in their general transmission patterns. The results for the first component S_0 of the Stokes vector \vec{S} are displayed in grayscale in Fig. 4.

3. Results

We now discuss the results obtained by applying our hybrid lattice Boltzmann algorithm to study the growth of blue phase domains inside cholesteric liquid crystals. To better analyse the growth dynamics, we restricted ourselves to the case of a thin slab of liquid crystal, and assumed periodic boundary conditions along the small direction, which we took along the z axis. This corresponds to assuming that the domain wall is locally straight and should approximate well the experimental situation in which the growing blue phase droplets are very large with respect to the unit cell size, so that locally they can be viewed as basically planar. In this geometry, which only requires few (16-32) lattice points along the z direction, we can study the time evolution of the order parameter and disclination network for timescale of up to seconds. In physical units, the size of one unit cell is about $0.5 \mu\text{m}$.

In our simulations, a fraction (typically) of the simulated lattice was initialised in a BPII structure, previously equilibrated at the selected values of κ and τ , whereas the rest of the lattice was initialised in the cholesteric phase. We first consider the case of low chirality and of a BPII domain growing inside a cholesteric phase ($\kappa = 1$, Fig. 1). It can be seen that the growth proceeds in a regular way: the BPII structure grows, as one would expect as its free energy is lower than that of the cholesteric (we are in a region in parameter space in which the cubic BPs are more advantageous structure than the cholesteric phase). The disclinations twist at the domain boundary to then merge into regular arrays of BPII unit cells. Their sizes are initially slightly larger than that of the initial template, but they rapidly equilibrate during growth to yield a virtually defect-free BPII lattice at the end of the simulations.

Increasing the chirality (Fig. 2), we observe an interesting phenomenon. The growth is much faster, and is more irregular at the surface. The twist at the advancing boundary can no longer be accommodated within the BP II lattice. Therefore, for large enough values of the chirality, it becomes more advantageous to switch to a completely different blue phase lattice, with hexagonal structure. This hexagonally ordered structure is different from the previously reported hexagonal phases, which were theoretically predicted to be stable only in weak electric fields [35]. The BP we report here is not, so far as we know, observed experimentally, but it would be interesting to understand whether it could be related to local ordering in blue phase III, which appear at a larger chirality than either BPI or BPII. It is quite possible anyway for such a phase to arise as a metastable intermediate.

The domain wall growth is very anisotropic. The results we have presented are with the cholesteric helix pointing along the y axis, perpendicular to the domain wall. We have performed additional simulations with different relative orientation between helix and domain wall. If the helix lies on the plane of the domain wall, we do not observe the transition to the hexagonally ordered structure. The anisotropy is also clear in the orientation we have chosen (Figs. 1 and 2), as the speed of advance of the domain boundary is not equal at both ends.

We have also performed simulations in which BPII was growing inside an isotropic phase at the same values of the reduced temperature. Again we find evidence of a transition between different BP lattices. At high values of the chiralities the “hexagonal” BP again forms, albeit through a different kinetic mechanism: instead of forming twisted disclination loops which are joined later on as within the cholesteric phase, the structure extends more regularly (Fig. 3). This reinforces the suggestion that at high chirality the hexagonal ordering of the BP lattice should be thermodynamically advantageous.

Finally, while Figs. 1, 2, 3 show the time evolution of the disclination line network, Fig. 4 gives the corresponding predicted optical patterns (one should keep in mind that the achievable resolution in an experiment would be smaller). It can be seen that the hexagonally ordered phase leaves a distinct signature from the BPII structure. Note that the hexagonal ordering is particularly evident in the larger corner spots in the optical pattern as well as generally in the $\sqrt{3} : 1$ aspect ratio of the rectangular pattern.

4. Conclusions

In conclusion, we have presented a hybrid lattice Boltzmann algorithm to solve the Beris-Edwards hydrodynamic equations of motion of cholesteric blue phases. The hybrid methodology mainly allows us to decrease the memory requirements, which in previous full LB approaches eventually limited the lattice sizes which could be reached.

We have shown that it is possible with this algorithm to perform supradomain simulations of blue phases, in which a large number of unit cells is simultaneously considered, as opposed to the previously reported single unit cell simulations, which assumed a regular lattice of disclination lines. In particular we have reported results on the growth of blue phase II domains in cholesterics, and shown that the growth dynamics is highly non-trivial. For low values of the chirality, the growth is regular and the blue phase forms without defects, whereas for large values of the chirality the growing region no longer has the structure of blue phase II, but attains a hexagonal ordering, and several defects appear at late times when the blue phase structure has invaded the whole computational domain. Finally, for very large values of the chirality, we observe a more regular hexagonal blue phases at late times. The switch between blue phase II and this hexagonal structure is due, in our interpretation, to the increasing twist which is developed at the domain wall, and which can no longer relax into a regular blue phase II unit cell. Our predicted transition from blue phase II to hexagonal structure appears for rather large values of the chirality, and it would be interesting to see whether these could be reached by the new temperature-stabilised blue phases. Also, it would be of interest to see whether this transition can be explained with extensions of the existing semi-analytical theories of blue phases, which are based on truncated expansions of the order parameter in Fourier components.

We acknowledge EPSRC grant EP/E045316/1 for funding, and G. P. Alexander and E. Orlandini for useful discussions and cpu time on Hector funded by EP/F054750/1.

References

- [1] S. Succi, *The Lattice Boltzmann Equation for Fluid Dynamics and Beyond*, Oxford University Press (2001).
- [2] B. M. Boghosian, *Computing in Science and Engineering*, **5**, 86 (2003).

- [3] K. Stratford, R. Adhikari, I. Pagonabarraga, J.-C. Desplat and M. E. Cates, *Science* **309**, 2198 (2005).
- [4] P. S. Clegg, *J. Phys.: Condens. Matt.* **20**, 113101 (2008).
- [5] M. R. Swift, E. Orlandini, W. R. Osborn and J. M. Yeomans, *Phys. Rev. E* **54**, 5041 (1996).
- [6] A. J. Wagner and J. M. Yeomans, *Phys. Rev. Lett.* **80**, 1429 (1998).
- [7] G. Gonnella, E. Orlandini and J. M. Yeomans, *Phys. Rev. Lett.* **78**, 1695 (1997).
- [8] A. G. Xu, G. Gonnella and A. Lamura, *Phys. Rev. E* **74**, 011505 (2006).
- [9] A. G. Xu, G. Gonnella and A. Lamura, *Physica A* **362**, 42 (2006).
- [10] C. Denniston, D. Marenduzzo, E. Orlandini and J. M. Yeomans, *Phil. Trans. R. Soc. Lond. A* **362**, 1745 (2004).
- [11] D. Marenduzzo, E. Orlandini, M. E. Cates and J. M. Yeomans, *Phys. Rev. E* **76**, 031921 (2007).
- [12] M. E. Cates, S. M. Fielding, D. Marenduzzo, E. Orlandini and J. M. Yeomans, *Phys. Rev. Lett.* **101**, 068102 (2008).
- [13] K. Stratford, J.-C. Desplat, P. Stansell and M. E. Cates, *Phys. Rev. E* **76**, 030501 (2007).
- [14] P. Stansell, K. Stratford, J.-C. Desplat, R. Adhikari and M. E. Cates, *Phys. Rev. Lett.* **96**, 085701 (2006).
- [15] A. N. Beris and B. J. Edwards, *Thermodynamics of Flowing Systems*, Oxford Science Publications (1994).
- [16] R. Adhikari and I. Pagonabarraga, paper in preparation.
- [17] D. C. Wright and N. D. Mermin, *Rev. Mod. Phys.* **61**, 385 (1989).
- [18] H. J. Coles and M. N. Pivnenko, *Nature* **436**, 977 (2005).
- [19] P. Pieranski, R. Barbet-Massin and P. E. Cladis, *Phys. Rev. A* **31**, 3912 (1985).

- [20] P. Pieranski, *Phys. Rev. Lett.* **84**, 2409 (2000).
- [21] P. Pieranski, *Europhys. Lett.* **81**, 66001 (2008).
- [22] A. Dupuis, D. Marenduzzo, and J. M. Yeomans, *Phys. Rev. E* **71**, 011703 (2005).
- [23] G. P. Alexander and J. M. Yeomans, *Phys. Rev. E* **74**, 061706 (2006).
- [24] A. Dupuis, D. Marenduzzo, E. Orlandini, and J. M. Yeomans, *Phys. Rev. Lett.* **95**, 097801 (2005).
- [25] G. P. Alexander and D. Marenduzzo, *Europhys. Lett.* **81**, 66004 (2008).
- [26] H. Grebel, R. M. Hornreich and S. Shtrickman, *Phys. Rev. A* **30**, 3264 (1984).
- [27] R. G. Larson, *The Structure and Rheology of Complex Fluids*, Oxford University Press, USA (1999).
- [28] C. Denniston, E. Orlandini, J. M. Yeomans, *Phys. Rev. E* **63**, 056702 (2001).
- [29] R. Adhikari, K. Stratford, M. E. Cates and A. J. Wagner, *Europhys. Lett.* **71**, 473 (2005).
- [30] We note that in principle when entering a body force, we should add a correction term in the second moment of the p_i 's, see for instance A. J. Wagner, *Phys. Rev. E* **74**, 056703 (2006). This may have a quantitative effect, although theoretically in our case the correction terms in the Chapman-Enskog expansion would be third order in gradients, and these are commonly neglected [28].
- [31] A. J. Wagner, *Int. J. Mod. Phys. B* **17**, 193 (2003).
- [32] E. Berggren, C. Zannoni, C. Chicolli, P. Pasini and F. Semeria, *Phys. Rev. E* **50**, 2929 (1994).
- [33] C.F. Bohren and D.R. Huffman, *Absorption and Scattering of Light by Small Particles*, Wiley, New York (1998).
- [34] R. Ondris-Crawford, E.P. Boyko, B.G. Wagner, J.H. Erdmann, *J. Appl. Phys.* **69**, 6380 (1991).

- [35] R.M. Hornreich, M. Kugler, S. Shtrikman, *Phys. Rev. Lett.* **54**, 2009 (1985).

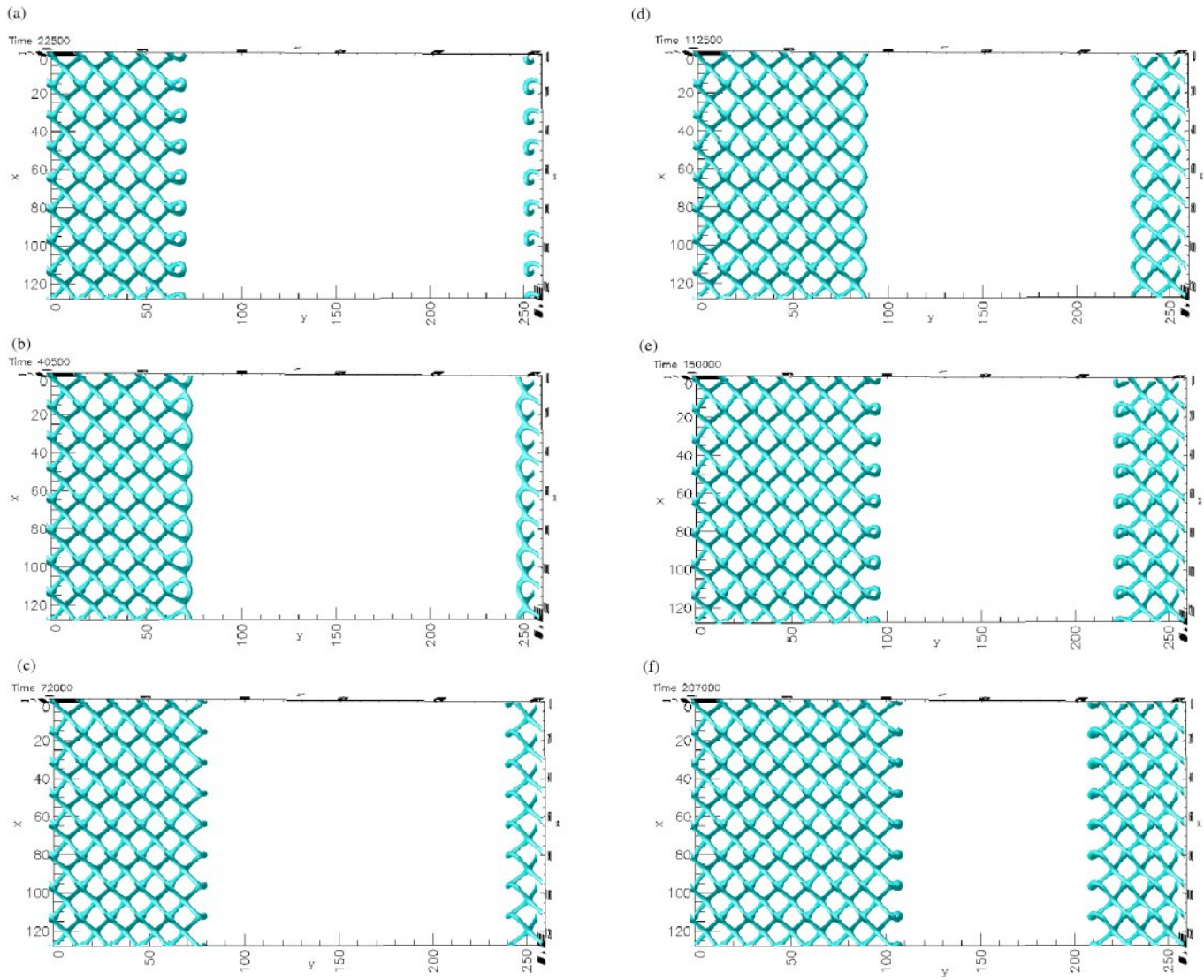


Figure 1: (a)-(f) Snapshots of the 2D projection of the disclination network of a growing BPII domain inside a cholesteric phase. Times (in simulation units) are shown in each of the panels. The chirality and reduced temperature were $\kappa = 1$ and $\tau = 0$ respectively.

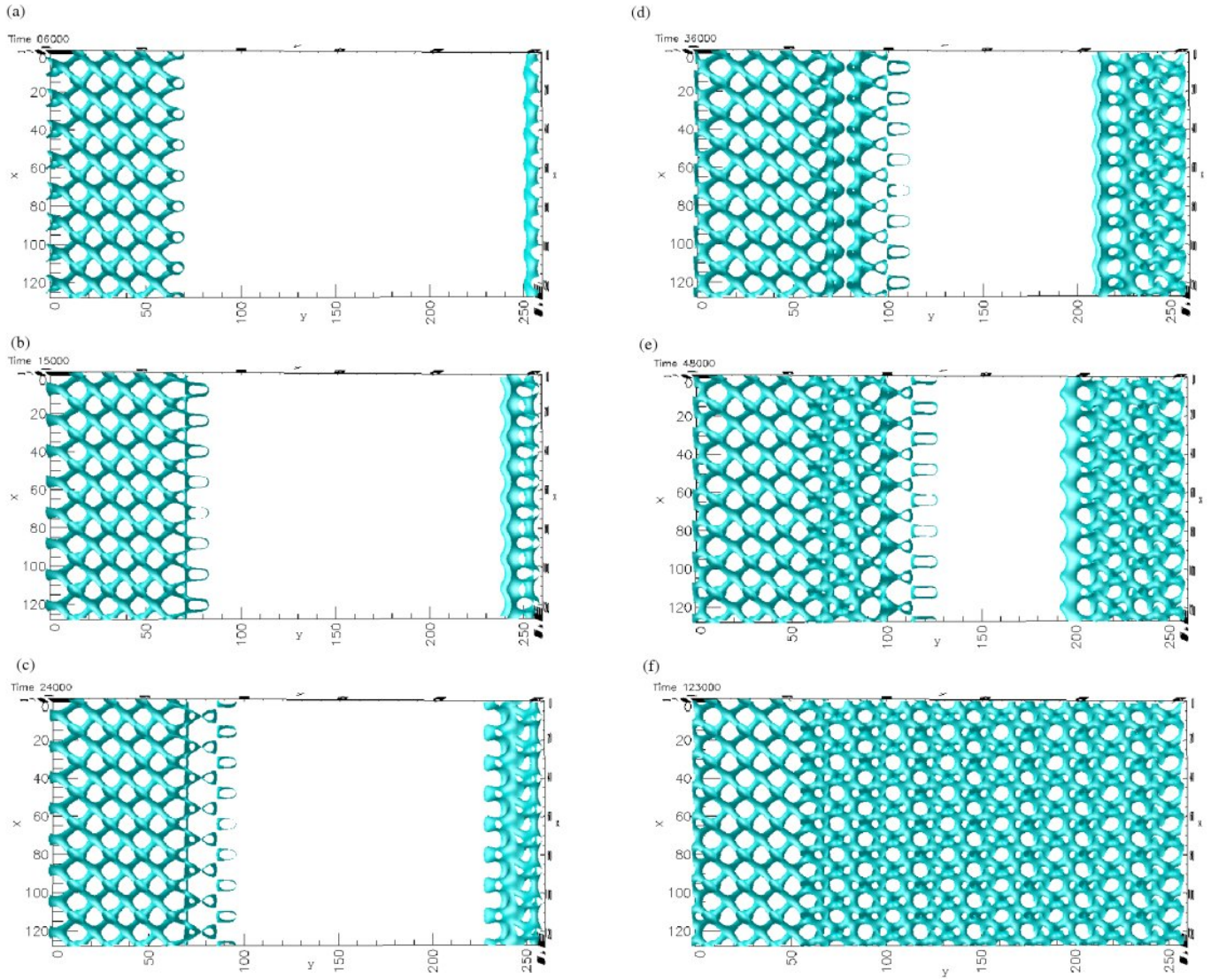


Figure 2: (a)-(f) Snapshots of the 2D projection of the disclination network of a growing BPII domain inside a cholesteric phase. Times (in simulation units) are shown in each of the panels. The chirality and reduced temperature were $\kappa = 2$ and $\tau = 0$ respectively.

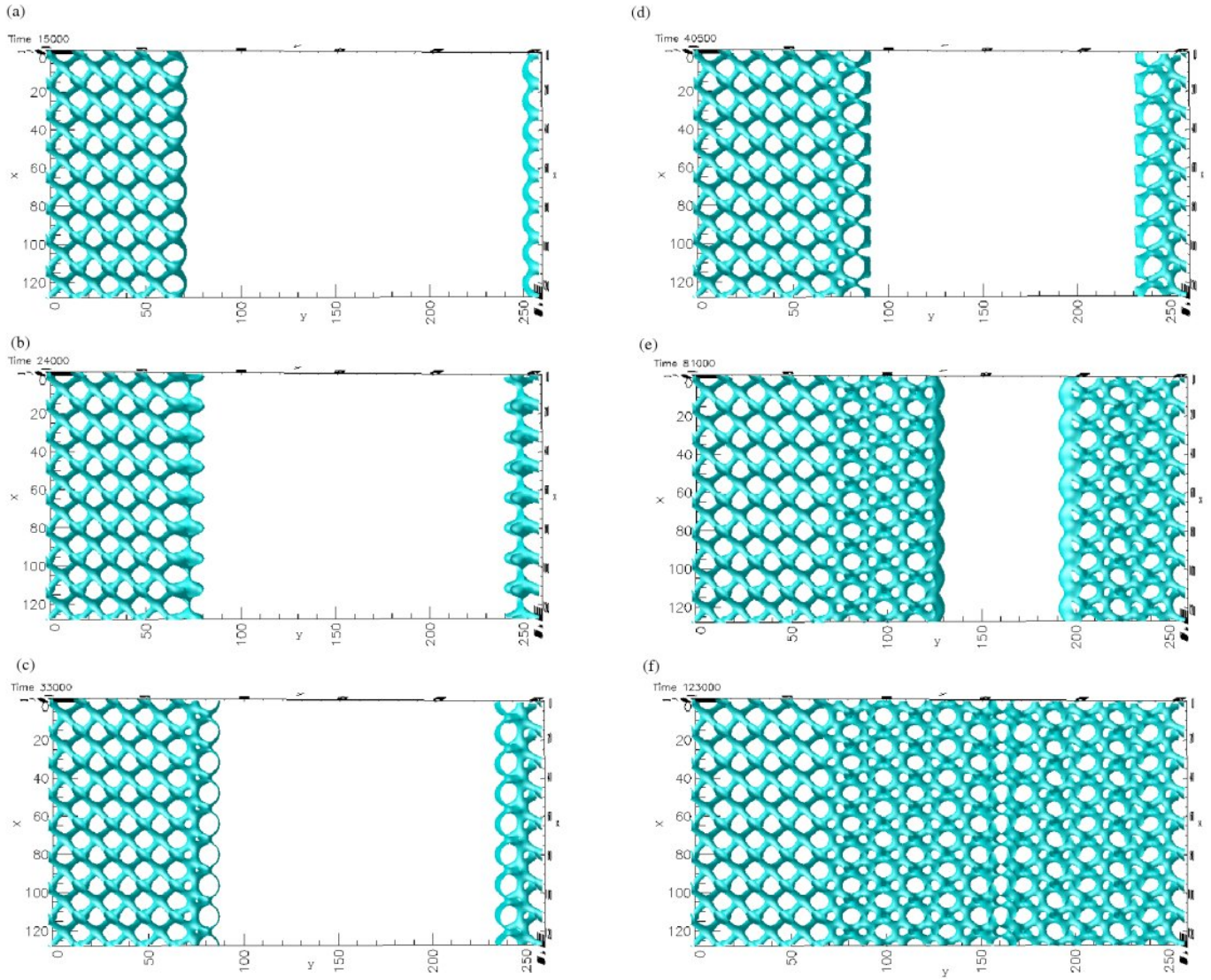


Figure 3: (a)-(f) Snapshots of the 2D projection of the disclination network of a growing BPII domain inside an isotropic phase. Times (in simulation units) are shown in each of the panels. The chirality and reduced temperature were $\kappa = 2$ and $\tau = 0$ respectively.

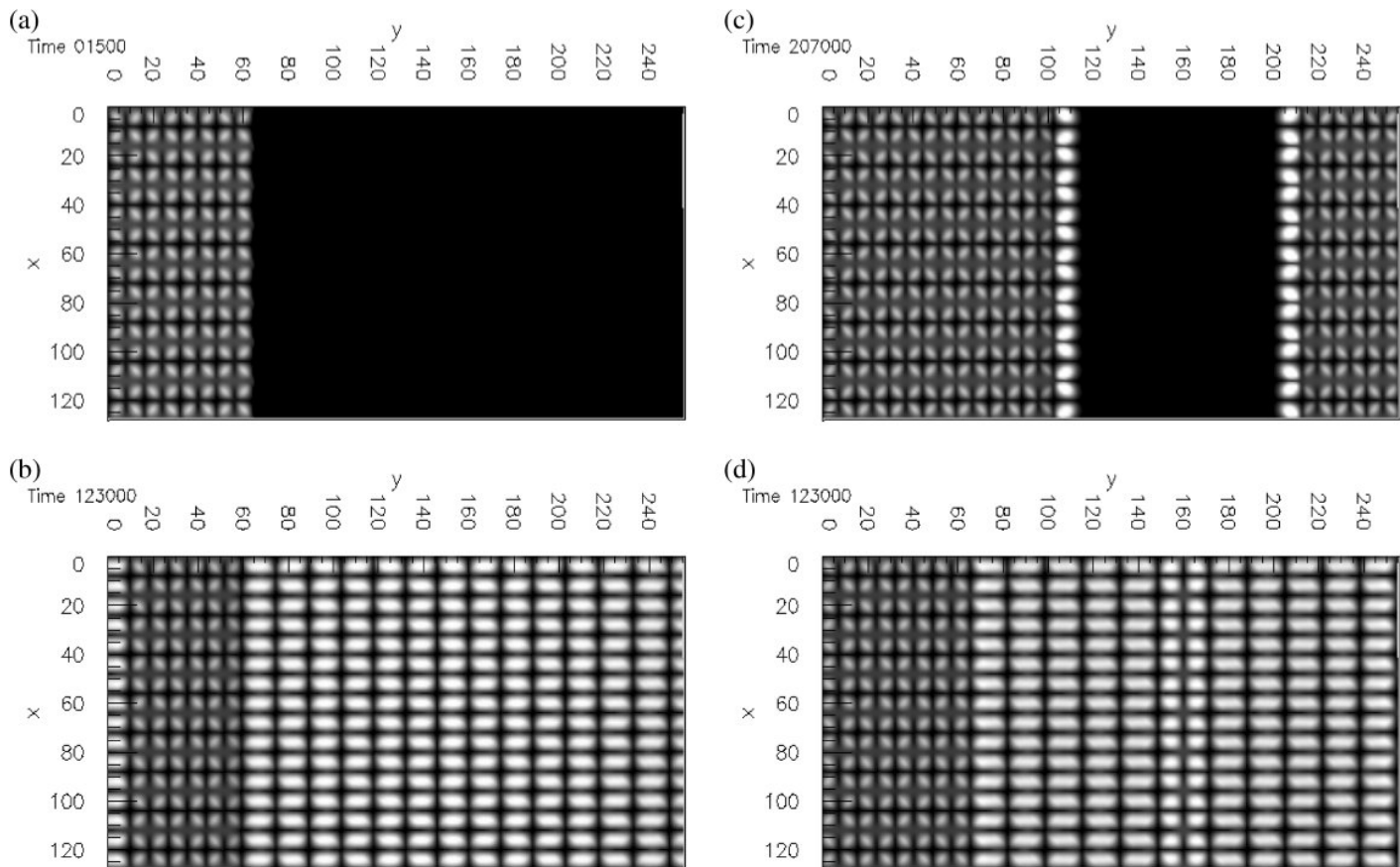


Figure 4: Predicted optical patterns for the (a) initial configuration, and final simulated configurations for (b) $\kappa = 1$ and a BPII in an initially cholesteric phase; (c) $\kappa = 2$ and a BPII in an initially cholesteric phase; (d) $\kappa = 2$ and a BPII in an initially isotropic